HIV-1 Fusion Peptide Decreases Bending Energy and Promotes Curved Fusion Intermediates

Stephanie Tristram-Nagle* and John F. Nagle*†
*Biological Physics Group, Department of Physics, and †Department of Biological Sciences, Carnegie Mellon University, Pittsburgh, Pennsylvania 15213

ABSTRACT A crucial step in human immunodeficiency virus (HIV) infection is fusion between the viral envelope and the T-cell membrane, which must involve intermediate membrane states with high curvature. Our main result from diffuse x-ray scattering is that the bending modulus K_C is greatly reduced upon addition of the HIV fusion peptide FP-23 to lipid bilayers. A smaller bending modulus reduces the free energy barriers required to achieve and pass through the highly curved intermediate states and thereby facilitates fusion and HIV infection. The reduction in K_C is by a factor of 13 for the thicker, stiffer 1,2-*sn*-dierucoylphosphatidylcholine bilayers and by a factor of 3 for 1,2-*sn*-dioleoylphosphatidylcholine bilayers. The reduction in K_C decays exponentially with concentration of FP-23, and the 1/e concentration is <1 mol % peptide/lipid, which is well within the physiological range for a fusion site. A secondary result is, when FP-23 is added to the samples which consist of stacks of membranes, that the distance between membranes increases and eventually becomes infinite at full hydration (unbinding); we attribute this both to electrostatic repulsion of the positively charged arginine in the FP-23 and to an increase in the repulsive fluctuation interaction brought about by the smaller K_C. Although this latter interaction works against membrane fusion, our results show that the energy that it requires of the fusion protein machinery to bring the HIV envelope membrane and the target T-cell membrane into close contact is negligible.

INTRODUCTION

Fusion of the membrane of enveloped viruses such as human immunodeficiency virus-type 1 (HIV-1) with the target T-cell is required for infection (1). In the case of HIV-1, the envelope glycoprotein gp160 contains two noncovalently bound subunits, gp120 and gp41 (2). After the initial docking step in which sites on the gp120 interact with the CD4 and chemokine receptors on the target membrane (3,4), the N-terminal hydrophobic region of the viral gp41 envelope protein is thought to provide the crucial perturbation of the target membrane that induces fusion of the viral and T-cell membranes, thus allowing the viral RNA to be injected into the host cell (5,6). The importance of the N-terminal 23 amino acids (FP-23) of gp41 has been shown by studies using synthetic FP-23; this short peptide is able to fuse and/or lyse liposomes and erythrocytes (7,8). In addition, mutations with a polar residue in the fusion peptide domain drastically reduce the fusogenic activities (9,10). Therefore, understanding the effects of the FP-23 peptide on membranes is an important step in HIV infection.

Membrane fusion is ubiquitous in healthy cells (1,11) as well as in different kinds of viral infection (12,13), and it is usually supposed that there are shared mechanisms and intermediate states, some of which are illustrated in Fig. 1. Starting from two flat membranes, a first intermediate (Fig. 1 *A*) involves dimples (also known as nipples) that bring the two membranes into close contact locally (14–16). Bending the membranes is presumed to cost a bending free energy that is paid for by conformational changes in proteins (12,13,15,16). The second intermediate shown in Fig. 1 *B* is the stalk that involves a topologically discontinuous transition from the contact intermediate. The stalk allows lipids from the contacting (proximal) monolayers to mix, which is an operational definition of hemifusion. There was an initial concern that the stalk would cost too much free energy, but it is now thought that a kinetically acceptable free energy of <40 kT (12,14,17) can be achieved in a modified stalk (14,18–20). Furthermore, if the contact intermediate causes the contact zone to be sufficiently dehydrated, the stalk free energy could be much smaller or stalk formation could even be spontaneous (21,22).

Another possible intermediate is a hemifusion diaphragm, shown in Fig. 1 *C*, that might grow from the stalk (1,12,16,23) and that would eventually break, involving another topological discontinuity that would lead to the fusion pore with an aqueous diameter $2r$ (illustrated in Fig. 1 *D*). It has been suggested that an extended diaphragm may not be a necessary intermediate (14,15) and that the stalk may lead directly, by a different topological discontinuity, to a prefusion pore with small value of the pore diameter $2r$ in Fig. 1 *D*. Subsequent growth into a fusion pore large enough to mix the contents of the two original cells or vesicles is expected to require considerable additional free energy (15,23). Regardless of uncertainties in the intermediates, the point of Fig. 1 for this article is that the bilayers or monolayers in these commonly accepted states have considerable curvature.

The broad strategy of our research is to study the effects of adding FP-23 to pure lipid bilayers in their most relevant, fully hydrated, fluid (liquid-crystalline) state. Although the

Submitted March 19, 2007, and accepted for publication May 18, 2007.

Address reprint requests to Stephanie Tristram-Nagle, Tel.: 412-268-3174; Fax: 412-681-0648; E-mail: stn@cmu.edu.

Editor: Thomas J. McIntosh.

0006-3495/07/09/2048/08 $2.00

doi: 10.1529/biophysj.107.109181

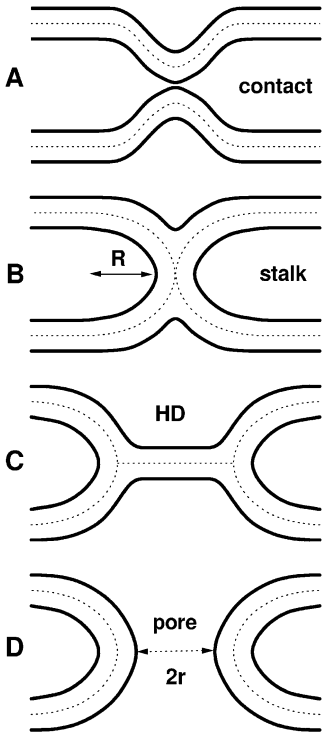

FIGURE 1 Well-known hypothetical fusion intermediates. Lipid bilayer surfaces are indicated by solid lines. Dotted lines in the hydrocarbon interior divide the bilayers into monolayers. (*A*) Contact of the virus and target membranes, (*B*) stalk that allows lipid mixing, (*C*) hemifusion diaphragm (*HD*), and (*D*) pore.

condition of full hydration has been difficult for quantitative structure determination, our recently developed technique that measures diffuse scattering has provided accurate structures of pure bilayers (24–27) and this provides the reference against which to compare the structural perturbations of peptides on bilayers. Our methodology provides the experimental form factors $F(q_z)$ of the bilayer, with and without peptides. Interpretation of the location of the peptide is nontrivial (28–30) and will not be attempted in this article. Diffuse x-ray scattering also provides the membrane bending modulus K_C (often written as κ in the literature), which measures how much energy is required to bend the membrane ($E = \frac{1}{2}K_C C^2$), where the curvature $C = R^{-1}$, and R is the radius of curvature.

In addition, the bulk, or compression, modulus B, which measures the overall interactions between two membranes in our samples is obtained. Indeed, it is necessary to obtain these two material moduli before the structural form factors $F(q_z)$ can be determined. Instead of just being a necessary prerequisite step, however, we suggest that the decrease that we observe in the bending modulus as FP-23 is added to lipid bilayers is a significant finding in its own right. As noted above and in Fig. 1, intermediate structures in the pathway to fusion involve highly strained and curved membranes, and the free energy required is proportional to the bending modulus, which in theoretical calculations has usually been taken from its values in pure lipid bilayers (12,14,16,17,19,21). A reduction in bending modulus of membranes with FP-23 incorporated lowers the free energies of the intermediates, thereby facilitating fusion.

MATERIALS AND METHODS

FP-23 and lipids

Synthetic fusion peptide FP-23 (AVGIGALFLGFLGAAGSTMGARS) was purchased from SynPep (Dublin, CA) at >90% purity, and FP-23 of higher purity (>95%) was purchased from the Peptide Synthesis Facility at the Pittsburgh Biotechnology Center; results were similar from both lots. The purity of both peptides was verified at the Center for Molecular Analysis at CMU using mass spectrometry. Lipids (1,2-*sn*-dioleoylphosphatidylcholine (DOPC) and 1,2-*sn*-dierucoylphosphatidylcholine (diC22:1PC)) were purchased from Avanti Polar Lipids (Alabaster, AL). Hexafluoroisopropanol (HIP) was used to make a stock solution of FP-23. HIP was high-performance liquid chromatography grade and was purchased from Aldrich Chemical (Milwaukee, WI).

Oriented sample preparation and hydration

Oriented samples were prepared using the rock-and-roll method (31). First, 4 mg peptide/lipid in neat HIP (200 μl) was deposited onto a flat 15 × 30 × 1 mm acid-cleaned silicon wafer, subjected to shear during evaporation of the organic solvent, and trimmed to 5 mm along the beam direction (for details see Tristram-Nagle (32)). Hydration was then carried out from water vapor in a thick-walled hydration chamber (25). Samples were studied as a function of hydration as monitored by the lamellar x-ray D-spacing. These D-spacings were compared to the fully hydrated D-spacing of peptide/lipid solutions in excess water in x-ray capillaries.

X-ray data collection

Oriented x-ray data were taken at the Cornell High Energy Synchrotron Source (CHESS) using the D1 station with wavelength 1.18 ± .016 Å. The flat samples were rotated from −3° to 7° in θ during the data collection. The beam was ~1 mm tall to fully cover the sample at all rotation angles and 0.2 mm wide to provide small angular divergence (<1.4×10^{-4} radian) in the horizontal direction. Total beam intensity was 10^9–10^{10} photons/s. The samples were shifted laterally after 2 min of x-irradiation to avoid beam-induced damage. Data were collected using a Medoptics charge-coupled device (CCD) with a 1024 × 1024 pixel array. More details of the typical setup are described by Kučerka et al. (25,26). To determine the degree of misorientation of bilayers (mosaic spread) on the silicon substrate, a rocking curve was collected by varying the angle of incidence through the Bragg angle θ in steps of .02° through the second order peak. Successive CCD images were collected, and the intensity of the second order Bragg reflection was plotted versus θ. This peak was fit with a Gaussian; the full width at half-maximum is reported as the mosaic spread in degrees. Fully hydrated *D*-spacings of samples in excess nanopure water (Barnstead, Dubuque, IA) were obtained in glass x-ray capillaries at 30°C using a Rigaku (The Woodlands, TX) RUH3R microfocus rotating anode equipped with a Xenocs (Sessenage, France) FOX2D focusing collimation optic; 5 min scans were collected using a Rigaku Mercury CCD detector; silver behenate (D = 58.367 Å) was used to calibrate the *S*-distance.

Thin layer chromatography

After scattering measurements, lipids were assayed for degradation using thin layer chromatography (TLC) with the solvent system chloroform/

methanol/7 M ammonium hydroxide (46:18:3, v/v). No lysolecithin formation was observed in samples of either pure lipids or mixtures of FP-23 with lipid when stained with a sensitive molybdic acid dye.

X-ray data analysis

The data analysis has been described previously (24,33) and will only briefly be reviewed here. The scattering intensity for a stack of oriented bilayers is the product $I(\mathbf{q}) = S(\mathbf{q})|F(q_z)|^2/q_z$, where $\mathbf{q} = (q_r, q_z)$, $S(\mathbf{q})$ is the structure interference factor, $F(q_z)$ is the bilayer form factor, and q_z^{-1} is the usual low-angle approximation to the Lorentz factor for oriented samples. The diffuse x-ray scattering is quasielastic, and the dynamic time range is very short; so the data represent the thermal average of many snapshots of the positional disorder in the sample. The appropriate theory is therefore an equilibrium statistical theory of smectic liquid crystals (34) that takes into account positional disorder with no inclusion of dynamics. The detailed theory includes the bilayer bending modulus K_C and the compression modulus B, which appear in the well-established fluctuational energy for smectic liquid crystals (34,35):

$$E_{fl} = \frac{1}{2}\int d\mathbf{r} \sum_{n=0}^{N-1} \{K_C[\Delta u_n(\mathbf{r})]^2 + B[u_{n+1}(\mathbf{r}) - u_n(\mathbf{r})]^2\}, \quad (1)$$

where n labels the membranes in a stack, $\boldsymbol{r}$ is the lateral position, and $u_n(\mathbf{r})$ is the deviation perpendicular to membrane from its average position, $\Delta u_n(\mathbf{r})$ is the curvature, and $u_{n+1}(\mathbf{r}) - u_n(\mathbf{r})$ is the fluctuation in the distance between neighboring bilayers from the average position. The term with the K_C factor is the bending energy, and the term with the B factor is the harmonic approximation to the energy of fluctuations in the distance between neighboring bilayers.

The membrane-membrane pair correlation functions follow from this statistical theory, and a computer program calculates the structure factor $S(\mathbf{q})$ for given values of K_C and B (33). Nonlinear least squares fitting of $S(\mathbf{q})$ to the data in the gray fitting boxes shown in Fig. 2 provides the best values of K_C and B. The fit is to the q_r dependence and is performed simultaneously for each of ~300 values of q_z in the fitting boxes. In addition to K_C and B, which are required to be the same for all values of q_z, the fit has two parameters for each q_z; one is a factor that gives $|F(q_z)|^2/q_z$ from which structure is determined, and the second is a small offset to compensate for imperfect background subtraction. The fitting boxes were chosen such that the data in the q_r direction are robust and not corrupted by the specular reflectivity that occurs near $q_r = 0$ nor by mosaic spread from the very strong $h = 1$ and $h = 2$ orders. The fitting box was chosen wide enough that the data go to zero at the high q_r edge of the fitting box as shown in Fig. 2.

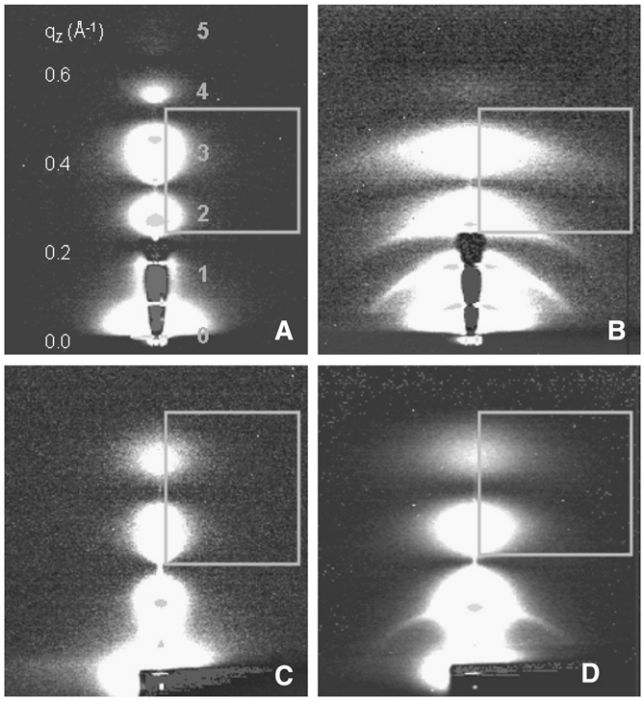

FIGURE 2 Some CCD images of scattering data from stacks of ~2000 membranes at 30°C of (*A*) diC22:1PC, (*B*) FP-23:diC22:1PC (1:15, $X = 0.0625$), (*C*) DOPC, and (*D*) FP-23:DOPC (1:17, $X = 0.056$). Dark pixels have low intensity, white pixels have intermediate intensity; and the highest intensities corresponding to diffraction peaks are shown by small gray spots within the white regions. The white regions define diffuse scattering lobes that are numbered in *A*. The vertical component of the scattering vector is q_z (perpendicular to the membranes), and the horizontal component is q_r (in-plane). The dark horizontal strip at the bottom of the images results from a semitransparent beam stop through which the main x-ray beam may be seen at $q_z = 0.0$. The narrow vertical dark strip in the center of frames *A* and *B* between $q_z = 0$ and ~0.25 $Å^{-1}$ is caused by another weaker attenuator through which the very strong first two Bragg orders can be seen as white notches or gaps near $q_z = 0.1$ and 0.2 $Å^{-1}$. The gray boxes are the fitting boxes within which the diffuse scattering theory described in Materials and Methods is fit to the data to obtain K_C and B. The flat samples were rotated between −3° and 7° relative to the beam during the 30-s (*A*), 40-s (*B*), or 60-s (*C* and *D*) exposure to sample evenly all of q-space that has nonzero intensity.

RESULTS

Fig. 2 shows the scattering intensity collected as CCD images at the CHESS synchrotron. These lobe-like diffuse data are caused by thermal fluctuations in fully hydrated stacks of lipid bilayers. When FP-23 (Fig. 2, *B* and *D*) is added to control lipids as described in Materials and Methods and hydrated, there are clearly differences compared to the pure lipid bilayers (Fig. 2, *A* and *C*). Most striking is loss of intensity in the smaller lobes at higher q_z. There are also significant changes in the widths of the lobes at lower q_z. A minor increase in width was due to increased mosaic spread (degree of misorientation). The sample in Fig. 2 *B* had a mosaic spread of 0.36° compared to 0.05° for the diC22:1PC control. The sample in Fig. 2 *D* had a mosaic spread of 0.24° compared to 0.05° for the DOPC control. Our analysis allowed us to include mosaic spread, but little difference in K_C was obtained until the mosaic spread exceeded 1°. More importantly, the width of the lobes increased due to changes in the material moduli K_C and B, as suggested by the grayscale images in Fig. 2. This widening is shown quantitatively in Fig. 3. However, the positions of the lobes and the minima between them along the q_z axis do not change substantially with addition of FP-23. Therefore, we estimate that any thinning of the bilayer thickness with addition of FP-23 is limited to ~0.1 nm.

Fig. 3 illustrates the goodness of the fit of the smectic liquid crystal theory to the primary data for one of the many values of q_z in the boxes shown in Fig. 2. This analysis provides values of K_C and B for each sample at a particular x-ray lamellar repeat spacing D. The values of K_C are plotted

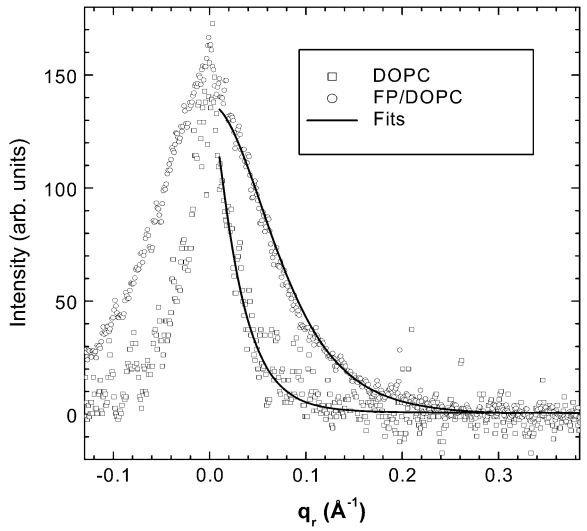

FIGURE 3 Normalized and background subtracted DOPC and FP-23/DOPC (1:17, $X = 0.056$) diffuse scattering data as a function of q_r at the position of the highly diffuse fifth order peak $q_z = 10\pi/D$ are shown by open symbols. The corresponding fits from the diffuse scattering theory are shown by black lines.

in Fig. 4 for the two lipid bilayers with and without FP-23 as a function of D. The D spacing is one indication of the water space between membranes, D_W, where the thickness of the bilayer D_B is subtracted from D as $D_W = D - D_B$. As expected, because K_C is a property just of individual membranes and not of the interactions between membranes in a stack, K_C does not vary significantly for any of the four samples within the range of D shown in Fig. 4, where there is adequate water to prevent close contact between membranes. (Further dehydration will subject the sample to enough osmotic pressure to significantly increase the thickness of the membranes (36), which would be expected to increase K_C.) It may be noted that very small decreases in relative humidity result in quite large decreases in D spacing (see Fig. 3 in Chu et al. (37)).

The most striking and important result shown in Fig. 4 is that K_C is greatly decreased by the addition of FP-23 to either lipid bilayer. In addition, larger D spacings were achieved as the relative humidity was increased when FP-23 was added compared to the pure lipids. The maximum D spacings that were obtained for pure lipid bilayers in oriented stacks hydrated from the vapor are almost as large as we obtained in multilamellar vesicles fully hydrated in bulk water (26), 70 Å for diC22:1PC and 63.7 Å for DOPC. In contrast, when $X >$ 0.02 mol fraction of FP-23 is added to DOPC, the D spacing in multilamellar vesicles in bulk water is undefined, that is, the vesicles are said to unbind. The large range of D spacings for oriented stacks with FP-23 shown in Fig. 4 was obtained by reducing the vapor pressure to exert osmotic pressure. The unbinding of the stack of bilayers in excess water implies that FP-23 affects the interactions between the membranes.

Fig. 5 reports values of K_C for varying concentrations of FP-23 with dimonounsaturated lipids of two different thicknesses. The hydrocarbon thickness of DOPC is 26.8 Å and that of diC22:1PC is 34.4 Å, and the total steric thickness of the bilayers is estimated by adding 18 Å for the two headgroup layers (26). It may first be noted that our values of K_C for the pure lipid bilayers DOPC and diC22:1PC agree very well with those obtained by Rawicz et al. (38), who used the completely different aspiration pipette technique, and the difference in the K_C values is quantitatively explained by their polymer brush model. As FP-23 is added to either lipid

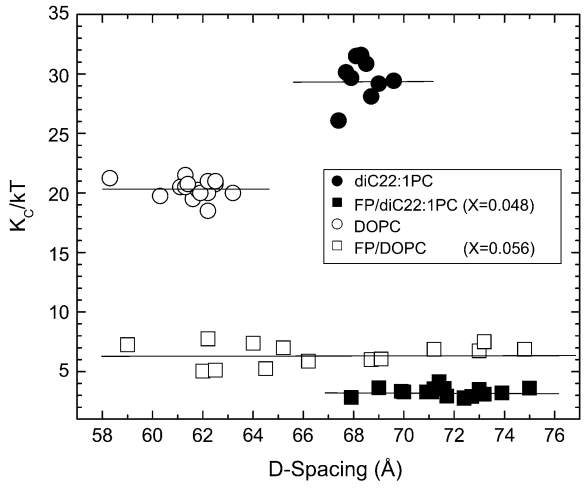

FIGURE 4 Values of bending modulus K_C, in units of thermal energy kT ($T = 303$ K), for the control lipid bilayers and for $X = 0.048$ and $X = 0.056$ mol fraction FP-23 in diC22:1PC and DOPC bilayers, respectively, as a function of lamellar repeat spacing D. D was systematically varied by changing the effective relative humidity using a tunable current through a Peltier device under the sample. The solid horizontal lines show average K_C/kT values, and uncertainties are estimated from the scatter of the data points.

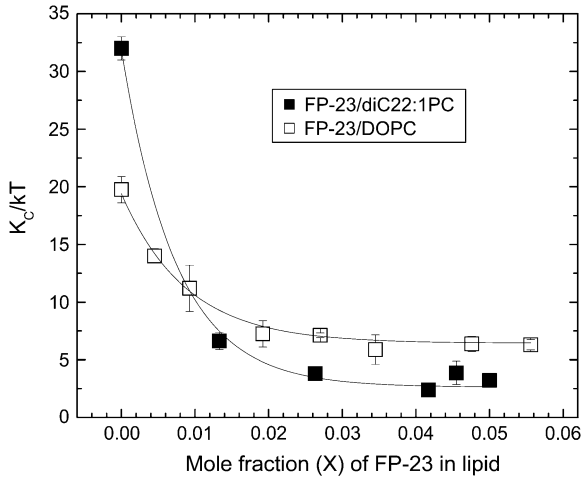

FIGURE 5 Effect on bending modulus K_C, in units of thermal energy kT, of adding FP-23 to diC22:1PC and to DOPC. The lines are exponential fits to the data with the parameters reported in Table 1.

bilayer, the bending modulus K_C decreases. We quantitate these results by fitting the data to an exponential decay $K_C(X) = K_{C/FP} + K_1 e^{-X/Xe}$, where $K_{C/FP}$ estimates the limiting value of K_C for large X. The values of X_e, $K_{C/FP}$, and $K_C(0) = K_{C/FP} + K_1$ are given in Table 1. FP-23 decreases $K_{C/FP}$ more relative to the initial $K_C(0)$ for diC22:1 than for DOPC.

We turn next to the B modulus, which is shown in Fig. 6. The B values are fitted as exponentials to many different hydration levels (D spacings) for several mole fractions X of FP-23 as shown in Fig. 6. The decay length D_e was obtained from the inverse of the slopes of the lines in Fig. 6 and its values are given in Table 2. In the soft confinement regime, the entropic fluctuation force has the form given by the first of the following equalities (35):

$$P_{fl} = \frac{d}{dD_W}\frac{kT\sqrt{B}}{2\pi\sqrt{K_C}} = \frac{kT}{4\pi\sqrt{K_C}}\frac{\sqrt{B_0}}{D_e}\exp\left(-\frac{\Delta D_W}{2D_e}\right). \quad (2)$$

The second equality in Eq. 2 uses the functional form for $B(D)$ obtained in Fig. 6, where B_0 is the reference value of the B modulus for a reference value of D_0, and $\Delta D_W = D - D_0$ is the difference in the water spacing from the same reference state. Equation 2 shows that P_{fl} increases as K_C decreases upon addition of FP-23, but the larger D_e in the denominator opposes the K_C effect. More importantly, the larger D_e in the exponential causes P_{fl} to increase for large D, as shown in Table 2.

As earlier noted in connection with Fig. 4, FP-23 caused both lipids to take up more water, which resulted in an increase in D spacing and eventual unbinding at full hydration. As is well known, finite D spacing involves a balance of forces; for uncharged bilayers these are an attractive van der Waals interaction (39) and two repulsive forces, the exponentially decaying hydration force (36), which is small for the large water spacings in our experiments, and an entropic force due to undulations of the individual bilayers (40). Also, FP-23 has an arginine residue and this adds an electrostatic repulsion to the previous interactions. Addition of only 5% negatively charged DPPA (dipalmitoylphosphatidic acid) has been reported to unbind DPPC bilayers (41). We have also found that addition of only 2% negatively charged DOPS (dioleoylphosphatidylserine) increases the D spacing of oriented stacks of DOPC by 12 Å and that 5% DOPS unbinds DOPC. The unbinding of the stack of bilayers upon addition of only 2% FP-23 is therefore likely due to both the electrostatic repulsion and the increased fluctuation repulsion. We also note that the electrostatic repulsion will undoubtedly cause deviations from exponential behavior for B when D_W is greater than the Guoy-Chapman length as has been shown for pure DOPS bilayers (42). However, for only 5% surface charge, the Guoy-Chapman length is 28 Å, which corresponds to $D = 73$ Å for DOPC with thickness 45 Å, so the exponential analysis in Fig. 6 that is valid for the soft confinement regime (43) may still be useful to diagnose the increase in fluctuation pressure in the preceding paragraph.

TABLE 1 Parameters for the fits to $K_C = K_{C/FP} + K_1 e^{-X/Xe}$ in Fig. 5

Sample	X_e	$K_{C/FP}$/kT	$K_C(0)$/kT
FP/DOPC	0.0088	6.5	20.5
FP/diC22:1PC	0.0074	2.5	31.8

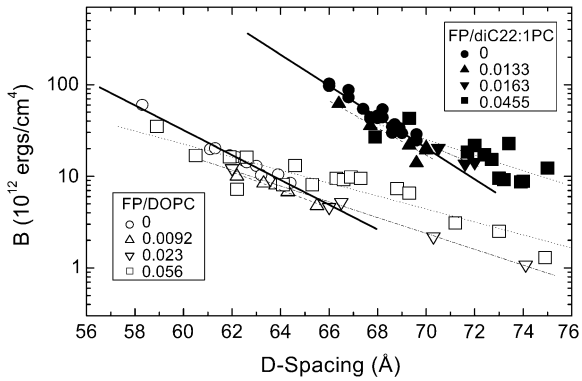

FIGURE 6 Compressibility modulus B as a function of lamellar repeat spacing D for FP-23 in DOPC (*open symbols*) and in diC22:1 (*solid symbols*) for several different mole fractions X of FP-23 given in the two figure legends. The lines are exponential fits to $B(D) = B_0\exp(-D/D_e)$ with D_e values given in Table 2. The solid lines are the exponential fits for the pure lipid controls, then dashed, dashed-dotted, and dotted are the exponential fits to the increasing mole fractions of FP-23.

DISCUSSION

Theories of fusion that estimate the free energies of intermediates use the bending modulus K_C of pure lipid bilayers, typically $K_C = 8 \times 10^{-13}$ ergs $= 20$ kT for DOPC bilayers and half that for monolayers in the stalk (12,14,16,17,19,21). Our result that K_C is reduced considerably by FP-23 suggests that smaller values of K_C should be considered in future. Smaller values will generally alleviate the concern that the free energy barriers in some models of fusion are too large (>40 kT) for kinetic competence. Of

TABLE 2 Interaction results

Lipid	FP-23 mol fraction	D_e (Å)	$P_{fl}(D_{W1})$ (10^3 dyn/cm^2)
DOPC	0	3.2	34
DOPC	0.0092	4.5	55
DOPC	0.023	5.0	70
DOPC	0.056	6.1	76
diC22:1PC	0	2.6	3.2
diC22:1PC	0.0133	2.9	9.1
diC22:1PC	0.0163	3.8	19
diC22:1PC	0.0455	5.1	45

D_e is the decay length of the B modulus in Fig. 6. $P_{fl}(D_{W1})$ is the fluctuation pressure at a water spacing $D_{W1} = 25$ Å.

course, this suggestion is only valid if our measured concentration X_e for significant reduction is not too large for the fusion process. The trimeric structure of gp41 (44) indicates that there are at least three FP-23 peptides near the fusion site. Our concentration $X_e = 0.008$ of FP-23 monomers means that three peptides define a domain of 375 lipids. Given a typical area/lipid of 0.7 nm^2, 375 lipids occupy two circular monolayer disks, each of radius 6.3 nm, a size that is comparable to the fusion site.

Let us relate this concentration even more specifically to the stalk intermediate shown in Fig. 1 *B*. In a stalk that has a semicircular profile with radius R along the normal to the fusing membranes and that is circular in the plane of the membranes, the contacting (proximal) monolayers have monolayer area $2\pi R^2[\pi(R + D_C)/R - 2]$, where R is the radius shown in Fig. 1 *B* and D_C (~1.5 nm) is the hydrocarbon thickness of a monolayer. This means that the effective radius R of the stalk can be as large as 4.5 nm and still attain the concentration X_e of FP-23. This is an ample stalk radius that allows room for the protein machinery to be contained between the target and viral envelope membranes. It is quantitatively the same size as the one sketched in Fig. 1 *B* if the thickness of the monolayers is set to D_C. This indicates that the FP-23 concentrations in this study are physiologically relevant.

Our measurements are necessarily performed on symmetric bilayers in which FP-23 is inserted equally in both monolayers. Of course, the peptide may also affect the spontaneous curvature ($C_S = R_S^{-1}$) of bilayers when inserted asymmetrically. Such spontaneous curvature may also help to reduce the free energy of some of the intermediates. However, the bending energy with spontaneous curvature, which is $(K_C/2)(C - C_S)^2$, still contains a factor of K_C; so its reduction also helps when the curvature of the intermediates is not perfectly matched to the spontaneous curvature. In this regard, it has been reported that several types of fusion peptides lower the phase transition temperature from flat liquid-crystalline systems to the highly curved inverted hexagonal phase, although this result alone does not indicate whether the peptide induces reduction of the bending modulus, increase of the negative spontaneous curvature, or some combination of the two, or whether the peptide preferentially partitions into stressed (''void'') regions in the H_{II} phase (45). Our technique, although silent about spontaneous curvature, nevertheless is definitive about the bending modulus.

The smectic liquid crystal theory that is the basis of the K_C data analysis assumes that the membranes are homogeneous in the lateral direction. For mole fraction $X = 0.05$, the average lateral distance between FP-23 molecules is ~2.5 nm, which is smaller than the lateral correlation length $\xi = (K_C/B)^{1/4}$ of the undulations in the sample, so it is reasonable to assume that the heterogeneity is at a small enough length scale to be statistically smeared in the analysis. However, as suggested in the previous paragraph, each FP-23 might reside primarily in one monolayer, and that could cause local spontaneous curvature in the bilayer. One might further speculate that the lateral locations of the FP-23 in the two monolayers in each bilayer are arranged in a ''staggered'' way along the plane of the bilayer, such that there is a smaller probability that both monolayers have an FP-23 at the same lateral location. Such an arrangement would curve the bilayer in opposite directions as a function of lateral displacement; this would be a wave, not one that is thermally activated but one that might decrease the value of K_C obtained from our analysis. If so, our main result that the bending modulus decreases could be construed as FP-23 inducing a local spontaneous curvature that might, if curved in the appropriate direction, also reduce the energy of curved fusion intermediates. However, the hypothesized staggered arrangement of FP-23 would, if sufficiently regular, produce in-plane scattering that we do not observe; so we favor our more straightforward interpretation that the bending modulus decreases.

Another concern is that the harmonic approximation that is intrinsic to the definition of K_C may break down for the highly curved intermediates in Fig. 1. As noted in the preceding paragraph, the modulus K_C is a macroscopic continuum concept relevant for average material properties and it does not take into account specific spatial accommodation that could arise from mixtures of molecules. These concerns have been addressed (17,21) by noting that the material moduli approach works well for inverted hexagonal lipid phases with comparable curvatures to the putative fusion intermediates; so it is certainly a useful first approximation. Nevertheless, with respect to the molecular point of view, we would suggest that the observed decrease in K_C due to FP-23 may also be thought of as indicating a weakening or disruption of the bilayer. Such disruption would facilitate the topologically discontinuous transitions that would have to occur when the stalk forms and again when the fusion pore forms. Returning to the continuum point of view, the thermally averaged root mean-square curvature scales as $(kT/K_C)^{1/2}/a_0$ where a_0 is an intermolecular distance, ~0.8 nm for lipids, so reduction in K_C allows for larger thermally activated fluctuations in curvature, and larger fluctuations facilitate topologically discontinuous transitions. Finally, we emphasize that the reduction in the bending modulus cannot be due to a simple thinning of the bilayer; to achieve a reduction factor of 13 in K_C for diC22:1PC would require the bilayer thickness to decrease by >2 nm, and that would require a large, and unobserved, expansion of the x-ray intensity pattern along q_z in Fig. 2.

Our study also obtains information about the interactions between membranes with FP-23. The first fusion intermediate must bring the membranes close together as in Fig. 1 *A*. However, FP-23 makes the repulsive fluctuation interaction stronger and it adds an electrostatic repulsion. Together these suffice to overwhelm the attractive van der Waals interaction at large distances. Therefore, the pure lipid bilayers, which maintain a finite interbilayer distance at full hydration, are driven much farther apart (this is often called unbinding) when FP-23 is added. This nonphysical unbinding of FP-23-loaded

bilayers emphasizes that the fusion peptide does not do everything. FP-23 is tethered to the transmembrane domain in the viral membrane, which prevents unbinding and, more importantly, the intervening protein machinery must then overcome all the repulsive interactions, of which there are three.

Of least concern is the electrostatic interaction because, unlike our experimental system where all neighboring bilayers should be charged, in viral fusion FP-23 would only attack the target T-cell; so there would not necessarily be any electrostatic repulsion with the neutral (or possibly even oppositely charged) viral membrane. Also, our experiments did not add salt, and its presence will screen the electrostatic interactions. Of greatest concern, as well recognized in the literature, is the short-range hydration force repulsion (36). Assuming a close contact zone with radius 1 nm, the energy required to achieve close contact against the hydration force is ~15 kT, which is a nonnegligible barrier for membrane contact. The repulsive fluctuation force whose strength we obtain is not usually considered. By similarly integrating the pressure given by Eq. 2 from 0 to infinity and using the values given in Table 2 and the value of B from Fig. 6, the energy to overcome the fluctuation pressure P_{fl} is ~2 orders of magnitude smaller than for the hydration force. Therefore, either with or without FP-23 and for both diC22:1PC and DOPC, P_{fl} presents a fairly minor additional hurdle to achieve the contact intermediate indicated in Fig. 1 *A* that then allows membrane fusion to proceed.

FP-23 likely plays several roles in viral fusion. One role could be to attach to the target T-cell so that conformational changes in gp41 could bring about the close contact indicated in Fig. 1 *A* (12,14). We suggest that the FP-23-induced reduction in the free energy of curved fusion intermediates is a previously unforeseen, and potentially important, additional role of FP-23 in HIV-1 infection.

The data for this study were taken on several runs at the D1 station, and we thank Drs. Detlef Smilgies and Arthur Woll for their help in setting up and Hee Kyoung Ko, Nelson Morales, and Jianjun Pan for help in collecting data. We also thank numerous colleagues for reading and commenting on the manuscript and especially Dr. M. Kozlov for insightful questions that led to a substantial addition to the Discussion.

This research was funded by grant GM 44976 from the General Medicine Institute of the National Institutes of Health. Synchrotron beam time was provided by the Cornell High Energy Synchrotron Source, which is funded by National Science Foundation grant DMR-0225180.

REFERENCES

1. Blumenthal, R., M. J. Clague, S. R. Durell, and R. M. Epand. 2003. Membrane fusion. *Chem. Rev.* 103:53–69.
2. Veronese, F. D., A. L. DeVico, T. D. Copeland, S. Oroszlan, R. C. Gallo, and M. G. Sarngadharan. 1985. Characterization of gp41 as the transmembrane protein coded by the $HTLV_{III}$/LAV envelope gene. *Science*. 229:1402–1405.
3. Lasky, A. L., G. Nakamura, D. H. Smith, C. Fennie, C. Shimasaki, E. Patzer, P. Berman, T. Gregory, and D. J. Capon. 1987. Delineation of a region of the hyman-immunodeficiency-virus type-1 gp120 glycoprotein critical for interaction with the CD4 receptor. *Cell*. 50:975–985.
4. Choe, H., M. Farzan, Y. Sun, N. Sullivan, B. Rollins, P. D. Porath, L. J. Wu, C. R. Mackay, G. LaRosa, W. Newman, N. Gerard, C. Gerard, and J. Sodroski. 1996. The beta-chemokine receptors CCR3 and CCR5 facilitate infection by primary HIV-1 isolates. *Cell*. 85: 1135–1148.
5. Gallaher, W. R. 1987. Detection of a fusion peptide sequence in the transmembrane protein of human-immunodeficiency-virus. *Cell*. 50: 327–328.
6. Bosch, M. L., P. L. Earl, K. Gargnoli, S. Picciafuoco, F. Giombini, F. Wong-Stall, and G. Franchini. 1989. Identification of the fusion peptide of primate immunodeficiency viruses. *Science*. 244:694–697.
7. Gordon, L. M., C. C. Curtain, Y. C. Zhong, A. Kirkpatrick, P. W. Mobley, and A. J. Waring. 1992. The amino-terminal peptide of HIV-1 glycoprotein-41 interacts with human erythrocyte-membranes—peptide conformation, orientation and aggregation. *Biochim. Biophys. Acta*. 1139:257–274.
8. Slepushkin, V. A., S. M. Andreev, M. V. Sidorova, G. B. Melikyan, V. B. Grigoriev, V. M. Chumakov, A. E. Grinfeldt, R. A. Manukyan, and E. V. Karamov. 1992. Investigation of human-immunodeficiency-virus fusion peptides—analysis of interrelations between their structure and function. *AIDS Res. Hum. Retroviruses*. 8:9–18.
9. Freed, E. O., E. L. Delwart, G. L. Buchschacher, and A. T. Panganiban. 1992. A mutation in the human-immunodeficiency-virus type-1 transmembrane glycoprotein-gp41 dominantly interferes with fusion and infectivity. *Proc. Natl. Acad. Sci. USA*. 89:70–74.
10. Mobley, P. W., A. J. Waring, M. A. Sherman, and L. M. Gordon. 1999. Membrane interactions of the synthetic N-terminal peptide of HIV-1 gp41 and its structural analogs. *Biochim. Biophys. Acta*. 1418:1–18.
11. Jahn, R., and T. C. Sudhof. 1999. Membrane fusion and exocytosis. *Annu. Rev. Biochem*. 68:863–911.
12. Chernomordik, L. V., and M. M. Kozlov. 2003. Lipid intermediates in membrane fusion: formation, structure, and decay of hemifusion diaphragm. *Annu. Rev. Biochem*. 72:175–207.
13. Tamm, L. K., J. Crane, and V. Kiessling. 2003. Membrane fusion: a structural perspective on the interplay of lipids and proteins. *Curr. Opin. Struct. Biol*. 13:453–466.
14. Kuzmin, P. I., J. Zimmerberg, Y. A. Chizmadzhev, and F. S. Cohen. 2001. A quantitative model for membrane fusion based on low-energy intermediate. *Proc. Natl. Acad. Sci. USA*. 98:7235–7240.
15. Cohen, F. S., and G. B. Melikyan. 2004. The energetics of membrane fusion from binding, through hemifusion, pore formation, and pore enlargement. *J. Membr. Biol*. 199:1–14.
16. Chernomordik, L. V., J. Zimmerberg, and M. M. Kozlov. 2006. Membranes of the world unite! *J. Cell Biol*. 175:201–207.
17. Malinin, V. S., and B. R. Lentz. 2004. Energetics of vesicle fusion intermediates: comparison of calculations with observed effects of osmotic and curvature stresses. *Biophys. J*. 86:2951–2964.
18. Lentz, B. R., D. P. Siegel, and V. Malinin. 2002. Filling potholes on the path to fusion pores. *Biophys. J*. 82:555–557.
19. Kozlovsky, Y., and M. M. Kozlov. 2002. Stalk model of membrane fusion: solution of energy crisis. *Biophys. J*. 82:882–895.
20. Markin, V. S., and J. P. Albanesi. 2002. Membrane fusion: stalk model revisited. *Biophys. J*. 82:693–712.
21. Kozlovsky, Y., A. Efrat, D. P. Siegel, and M. M. Kozlov. 2004. Stalk phase formation: effects of dehydration and saddle splay modulus. *Biophys. J*. 87:2508–2521.
22. Yang, L., and H. W. Huang. 2002. Observation of a membrane fusion intermediate structure. *Science*. 297:1877–1879.
23. Chernomordik, L. V., and M. M. Kozlov. 2005. Membrane hemifusion: crossing a chasm in two leaps. *Cell*. 123:375–382.
24. Liu, Y., and J. F. Nagle. 2004. Diffuse scattering provides material parameters and electron density profiles of biomembranes. *Phys. Rev. E*. 69:040901.

25. Kučerka, N., Y. Liu, N. Chu, H. I. Petrache, S. Tristram-Nagle, and J. F. Nagle. 2005a. Structure of fully hydrated fluid phase DMPC and DLPC lipid bilayers using x-ray scattering from oriented multilamellar arrays and from unilamellar vesicles. *Biophys. J.* 88:1–12.

26. Kučerka, N., S. Tristram-Nagle, and J. F. Nagle. 2005b. Structure of fully hydrated fluid phase lipid bilayers with monounsaturated chains. *J. Membr. Biol.* 208:193–202.

27. Kučerka, N., S. Tristram-Nagle, and J. F. Nagle. 2006. Closer look at structure of fully hydrated fluid phase DPPC bilayers. *Biophys. J.* 90:L83–L85.

28. Hristova, K., W. W. Wimley, V. K. Mishra, G. M. Anantharamiah, J. P. Segrest, and S. H. White. 1999. An amphipathic alpha-helix at a membrane interface: a structural study using a novel x-ray diffraction method. *J. Mol. Biol.* 290:99–117.

29. Huang, H. W., and Y. Wu. 1991. Lipid-alamethicin interactions influence alamethicin orientation. *Biophys. J.* 60:1079–1087.

30. Bradshaw, J. P., M. J. M. Darkes, J. Katsaras, and R. M. Epand. 2000. Neutron diffraction studies of viral fusion peptides. *Physica B.* 276–278:495–498.

31. Tristram-Nagle, S., R. Zhang, R. M. Suter, C. R. Worthington, W.-J. Sun, and J. F. Nagle. 1993. Measurement of chain tilt angle in fully hydrated bilayers of gel phase lecithins. *Biophys. J.* 64:1097–1109.

32. Tristram-Nagle, S. 2007. Preparation of oriented, fully hydrated lipids samples for structure determination using x-ray scattering. *In* Methods in Molecular Biology, Vol. 400: Methods in Membrane Lipids. A. M. Dopico, editor. Humana Press, Totowa, NJ. 63–75.

33. Lyatskaya, Y., Y. Liu, S. Tristram-Nagle, J. Katsaras, and J. F. Nagle. 2001. Method for obtaining structure and interactions from oriented lipid bilayers. *Phys. Rev. E.* 63:0119071–0119079.

34. DeGennes, P. G., and J. Prost. 1995. The Physics of Liquid Crystals. Oxford University Press, New York.

35. Petrache, H. I., N. Gouliaev, S. Tristram-Nagle, R. Zhang, R. M. Suter, and J. F. Nagle. 1998. Interbilayer interactions from high-resolution x-ray scattering. *Phys. Rev. E.* 57:7014–7024.

36. Rand, R. P., and V. A. Parsegian. 1989. Hydration forces between phospholipid bilayers. *Biochim. Biophys. Acta.* 988:351–376.

37. Chu, N., N. Kučerka, Y. Liu, S. Tristram-Nagle, and J. F. Nagle. 2005. Anomalous swelling of lipid bilayer stacks is caused by softening of the bending modulus. *Phys. Rev. E.* 71:041904.

38. Rawicz, W., K. C. Olbrich, T. J. McIntosh, D. Needham, and E. Evans. 2000. Effect of chain length and unsaturation on elasticity of lipid bilayers. *Biophys. J.* 79:328–339.

39. Parsegian, V. A. 2006. Van der Waals Forces. Cambridge University Press, New York.

40. Helfrich, W. 1973. Elastic properties of lipid bilayers—theory and possible experiments. *Z. Naturforsch.* 28:693–703.

41. McIntosh, T. J., and S. A. Simon. 1996. Adhesion between phosphatidylethanolamine bilayers. *Langmuir.* 12:1622–1630.

42. Petrache, H. I., S. Tristram-Nagle, K. Gawrisch, D. Harries, V. A. Parsegian, and J. F. Nagle. 2004. Structure and fluctuations of charged phosphatidylserine bilayers in the absence of salt. *Biophys. J.* 86:1574–1586.

43. Podgornik, R., and V. A. Parsegian. 1992. Thermal mechanical fluctuations of fluid membranes in confined geometries—the case of soft confinement. *Langmuir.* 8:557–562.

44. Hamburger, A. E., S. Kim, B. D. Welch, and M. S. Kay. 2005. Steric accessibility of the HIV-1 gp41 N-trimer region. *J. Biol. Chem.* 280: 12567–12572.

45. Epand, R. M., and R. F. Epand. 2000. Modulation of membrane curvature by peptides. *Biopolymers.* 55:358–363.